EPJ Applied Metamaterials

RESEARCH ARTICLE

OPEN ACCESS

Reflection and transmission of nanoresonators including bi-isotropic and metamaterial layers: opportunities to control and amplify chiral and nonreciprocal effects for nanophotonics applications

Evgenii Starodubtsev[*]

Gomel State Technical University, October ave. 48, Gomel 246746, Belarus

Abstract. Electromagnetic waves reflected from and transmitted through the multilayer nanoresonators including the main layer made of a bi-isotropic material or metamaterial sandwiched between dielectric, epsilon-near-zero or metallic spacer layers have been analytically modeled. The numerical and graphical analysis, based on the exact solution of the electromagnetic boundary problem, confirms opportunities to use such nanoresonators as utracompact polarization converters. The proposed systems are characterized by wide ranges of parameters and significantly reduced (subwavelength) thicknesses. The spacer layers can provide modification, control, and amplification of chiral and nonreciprocal effects for the reflected and transmitted radiation. The concept can be realized for various geometries of dielectric, epsilon-near-zero, metallic, bi-isotropic, metamaterial layers and used to develop new ultrathin, large area, and relatively easy-to-manufacture polarization and other devices for nanophotonics.

1 Introduction

The present paper is the second of two ones (the first is [1] where the detailed problem statement and general analytical model were discussed) devoted to the modeling of optical properties of the plane-layered nanoresonators including the main layer made of a bi-isotropic material or metamaterial (MM) sandwiched between pairs of dielectric, epsilon-near-zero (ENZ) or metallic spacer layers. Such one-dimensional nanometric systems (that are relatively easy to realize using modern thin film and nanocomposite technologies) demonstrate the optical properties that can be of interest for many nanophotonics applications. The main goal of both works is to investigate chiral and nonreciprocal effects in the systems of subwavelength thicknesses, possibilities to control and "amplify'' these effects by varying geometry and materials of the nanoresonator components, exciting radiation characteristics. There is a large number of both classical (e.g. [2–5]) and recent (see, e.g. [6–10] and numerous references in these papers) works in the field of chiral natural (gyrotropic) and artificial media. However, new

opportunities, arising from the rapid development of electrodynamics and technology of electromagnetic MMs [1,11–21], require further investigations and these opportunities are seemed to be very perspective for various applications of such media.

This paper uses the analytical model proposed in [1] and based on the accurate solution of the corresponding boundary electromagnetic problem for monochromatic waves, to investigate the features of reflected and transmitted radiation (the main properties of the proper waves inside of the system were considered in [1]). The present paper includes the detailed numerical and graphical analysis of the energy and polarization characteristics of the waves outside of the nanoresonator pointing to the new possibilities for applications of such systems as ultrathin polarization and phase converters, filters, modulators, metasurfaces and other components of nanophotonics devices.

Let us note that the investigated in the work reflection and transmission characteristics of the nanoresonators with absorbing bi-isotropic and MM layers of subwavelength thicknesses, apparently, have not yet been considered in detail (in contrast to the investigations of classical "macroscopic" chiral and nonreciprocal layered systems,

* e-mail: starodub@tut.by

e.g. [3–5]). Primarily, we consider the new features of the bi-isotropic effects in reflection and transmission (for both intensity and polarization characteristics) of such multilayers due to the "addition" of different (dielectric, ENZ, metallic, MM) components to the ultrathin layered systems.

The work has the following structure. For the sake of completeness, the brief problem statement, the analytical model description and main results from [1] (used for the numerical analysis in the present work) are given in Section 2. Main parameters and dependences for the numerical analysis are considered in Section 3. The polarization and intensity characteristics of the waves reflected from and transmitted through the nanoresonator are investigated in Sections 4 and 5, respectively. Special attention is paid to the analysis of the polarization effects of birefringence, dichroism, nonreciprocity and clarification of the conditions when it is possible to control such effects and "optimize" their characteristics by changing parameters of the nanoresonator and exciting radiation. In doing so, the cases of both "conventional" and MM components of the system are considered and compared. Section 6 includes the discussion of the obtained results and summarizes the paper.

2 Statement of the problem and general relations

We consider the interaction of an electromagnetic plane monochromatic wave with a layered system under oblique incidence [1]. A geometry of the multilayer and the corresponding electromagnetic boundary problem is illustrated in Figure 1. The layers have thicknesses $d_{1,2,3}$ (further lower indexes, $l = 0, 1, 2, 3, 4$ relate to the quantities characterizing the materials of the superstrate, multilayer components, and substrate, respectively). The superstrate and substrate media are assumed to be isotropic and semi-infinite (optically thick). So, there is only a transmitted wave inside of the substrate. Coordinate axis Z is perpendicular to the boundaries of the layers, plane XZ is the incidence plane. The relative intensities of the incident, reflected, and transmitted waves, I_{in}, I_r, I_t, and polarization characteristics of these waves are considered at boundaries $z = 0$ and $z = d_1 + d_2 + d_3$ (Fig. 1).

The materials of media 0, 1, 3, 4 are supposed to be isotropic, they are characterized by scalar dielectric permittivities $\varepsilon_{0,1,3,4}$ and magnetic permeabilities $\mu_{0,1,3,4}$. We assume that media 0, 4 (1, 2, 3) are non-absorbing (absorbing), correspondingly. Thus, quantities $\varepsilon_{0,4}$, $\mu_{0,4}$ are real and $\varepsilon_{1,2,3}$, $\mu_{1,2,3}$ are complex in the general case. According to the phase multiplier choice for the fields in the system [1] as $\exp\left[i\left(k_1 x + k_3 z\right) - i\omega t\right]$ ($\boldsymbol{k} = (k_1, 0, k_3)$ is a wave vector) and the causality conditions, the imaginary parts of permittivities and permeabilities for all the multilayer components are positive. The real parts of these quantities can be both positive and negative, so, we also consider the cases when the media are MMs. Denotations

$$a' = \operatorname{Re}(a),\ a'' = \operatorname{Im}(a)$$
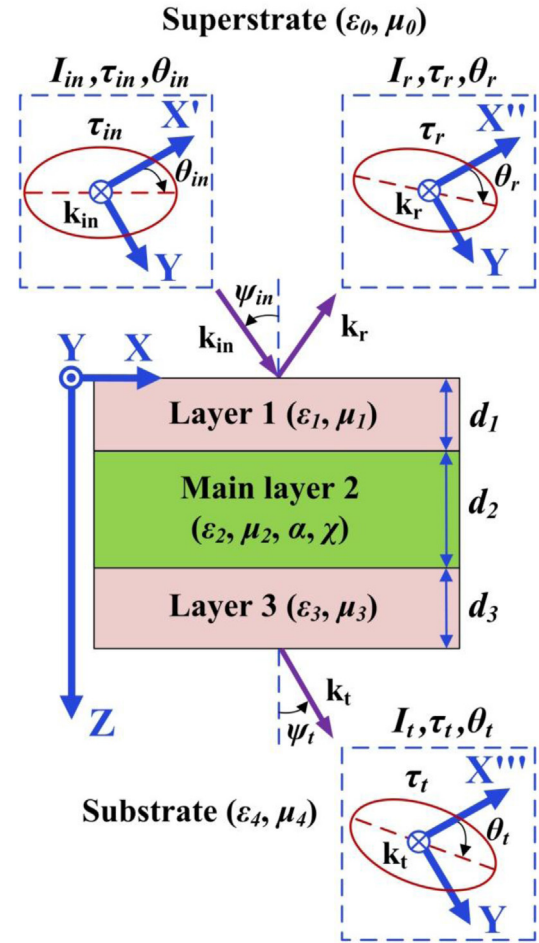

Fig. 1. The multilayer scheme and geometry of the corresponding electromagnetic boundary problem. The superstrate and substrate media are isotropic and semi-infinite. The multilayer includes spacer layers 1, 3 with thicknesses $d_{1,3}$, whose electromagnetic properties correspond to isotropic media (in particular, ENZ MMs), and the main bi-isotropic layer 2 with thickness d_2. Relative intensities I_{in}, I_r, I_t, ellipticities τ_{in}, τ_r, τ_t, polarization azimuths θ_{in}, θ_r, θ_t, and wave vectors $\boldsymbol{k_{in}}$, $\boldsymbol{k_r}$, $\boldsymbol{k_t}$ correspond to the incident, reflected, and transmitted waves, ψ_{in} and ψ_t are the angles of incidence and refraction, respectively. The fields inside of the multilayer are not shown. The inserts bounded by dotted lines illustrate orientations of the major axes of polarization ellipses of the incident, reflected and transmitted waves in the corresponding phase planes X′Y, X″Y, X‴Y, respectively. Additional notation is given in the main text.

are used as well for the real and imaginary parts of scalar or vector quantities.

For the homogeneous incident, reflected and transmitted waves in the non-absorbing superstrate and substrate media, the real angles of incidence (reflection), ψ_{in}, and refraction, ψ_t, are used (Fig. 1). These waves are assumed to be elliptically polarized in the general case. Orientations of the major axes of polarization ellipses (for the corresponding vectors of electric field strengths) in the related phase planes X′Y, X″Y, X‴Y are determined by angles θ_{in}, θ_r, θ_t, respectively (see the inserts in Fig. 1).

The main layer material is bi-isotropic and it is described by the constitutive relations including cross magneto-dielectric terms [2–5]: $\boldsymbol{D} = \varepsilon\boldsymbol{E} + (\chi + i\alpha)\,\boldsymbol{H}$, $\boldsymbol{B} = \mu\boldsymbol{H} + (\chi - i\alpha)\,\boldsymbol{E}$, where scalar (complex, in general) quantities $\varepsilon = \varepsilon_2$, $\mu = \mu_2$, α, χ (Fig. 1) are dielectric permittivity, magnetic permeability, chirality and non-reciprocity parameters, respectively. In the particular cases $\alpha \neq 0$, $\chi = 0$ and $\alpha = 0$, $\chi \neq 0$, these constitutive relations correspond to chiral (or naturally gyrotropic) and Tellegen's media [2–5].

To investigate numerically energy and polarization characteristics of the reflected and transmitted waves (Fig. 1), we use the previous analytical results [1]. The relative intensities of the reflected (at the boundary $z = 0$) and transmitted (at $z = d_1 + d_2 + d_3$) radiation are determined by the expressions

$$I_r = \frac{\left|a_0^-\right|^2 \varepsilon_0\mu_0 + \left|b_0^-\right|^2\eta_0^2}{\left|a_0^+\right|^2\varepsilon_0\mu_0 + \left|b_0^+\right|^2\eta_0^2},$$

$$I_t = \frac{\sqrt{\varepsilon_4/\mu_4}\left(\left|a_4^+\right|^2\varepsilon_4\mu_4\eta_4^{-2} + \left|b_4^+\right|^2\right)}{\sqrt{\varepsilon_0/\mu_0}\left(\left|a_0^+\right|^2\varepsilon_0\mu_0\eta_0^{-2} + \left|b_0^+\right|^2\right)}, \qquad (1)$$

where complex scalars $a_0^\pm$, $b_0^\pm$, a_4^+, b_4^+ characterize the fields in the media $\nu = 0, 4$ (Fig. 1) according to the relations

$$\boldsymbol{E}_v^\pm = \left(a_v^\pm, b_v^\pm, \mp m_1 a_v^\pm/\eta_v\right),$$
$$\boldsymbol{H}_v^\pm = \mu_v^{-1}(\mp \eta_v b_v^\pm, \pm \varepsilon_v\mu_v a_v^\pm/\eta_v, m_1 b_v^\pm). \quad (2)$$

In equations (2), the general for all the waves phase factor $\exp\left[ik_0\left(m_1 x \pm \eta_v z\right) - i\omega t\right]$ is omitted, $\eta_v = \sqrt{\varepsilon_v\mu_v - m_1^2}$ (choosing $\eta_v'' > 0$), $\boldsymbol{m} = (m_1,\ 0,\ m_3) = \boldsymbol{k}/k_0$ is a complex normalized wave vector or so called refraction vector [2] (k_0 is the wave number for vacuum), the upper indexes "+" and "−" correspond to the quantities describing transmitted ($\nu = 4$) and reflected ($\nu = 0$) proper waves.

Quantities a_0^-, b_0^- for the reflected wave in the superstrate and a_4^+, b_4^+ for the transmitted wave in the substrate are determined from the boundary problem solution using the given parameters a_0^+, b_0^+, m_1 characterizing the incident wave [1]:

$$a_0^+ = WE[\cos(\theta_{in}) - i\tau_{in}\sin(\theta_{in})]\cos(\psi_{in}),$$

$$b_0^+ = WE[\sin(\theta_{in}) + i\tau_{in}\cos(\theta_{in})], \qquad (3)$$

where $W = \left(1 + \tau_{in}^2\right)^{-0.5}$, $E = +\sqrt{8\pi I_{in}/\left(c\varepsilon_0^{0.5}\right)}$, c is the speed of light in vacuum, τ_{in} and I_{in} are ellipticity and intensity of the incident wave ($\tau_{in} = 0$ for linear and $\tau_{in} = +1$ for right and $\tau_{in} = -1$ for left circular polarizations), θ_{in} is an

angle between the incidence plane (XZ) and the major axis of polarization ellipse lying in the phase plane of the incident wave, ψ_{in} is the incidence angle (Fig. 1).

The polarization parameters of the reflected and transmitted waves are determined by the relations of the components of these waves in the corresponding phase planes $X''Y$ and $X'''Y$ (Fig. 1) [1]:

$$\xi_r = \frac{(\boldsymbol{E}_r)_Y}{(\boldsymbol{E}_r)_{X''}} = -\frac{b_0^-\cos(\psi_{in})}{a_0^-},$$

$$\xi_t = \frac{(\boldsymbol{E}_t)_Y}{(\boldsymbol{E}_t)_{X'''}} = \frac{b_4^+\cos(\psi_t)}{a_4^+}, \qquad (4)$$

where ψ_{in} and ψ_t are the incidence and refraction angles (Fig. 1), $\cos(\psi_t) = \sqrt{1 - \varepsilon_0\mu_0\sin^2(\psi_{in})/(\varepsilon_4\mu_4)}$. Using the approach [2], parameters $\xi_{r,t}$ determine ellipticities $\tau_{r,t}$ and polarization azimuths $\theta_{r,t}$ (Fig. 1) of the reflected and transmitted waves according to the expressions:

$$\tau^2 = \left(1 - \sqrt{T}\right)/\left(1 + \sqrt{T}\right),$$

$$T = 1 - 4\text{Im}^2(\xi)/\left(1 + |\xi|^2\right)^2,$$

$$tg(\theta) = \text{Re}\left(\xi/\sqrt{1 + \xi^2}\right)/\text{Re}\left(1/\sqrt{1 + \xi^2}\right),$$

where $\xi = \xi_{r,t}$, $\theta = \theta_{r,t}$. In these expressions, we choose $\tau > 0$ if $\xi'' > 0$ (right polarization), $\tau < 0$ if $\xi'' < 0$ (left polarization), $\tau = 0$ ($\xi'' = 0$) for linear polarization. The detailed description of the analytical model used here for the numerical and graphical analysis was given in [1].

The used analytical model is based on the assumptions considered in detail in [1]. In particular, the frequency dispersion of the electromagnetic parameters characterizing layer materials is not taken into account explicitly in the work. Instead, we consider below some "typical" values of parameters of different material layers that are characteristic for wide frequency ranges and can be realized using modern nanocomposite technologies. Such approach is caused by the main goal of the numerical analysis below, that is to confirm and illustrate (for specific and typical data) the opportunities to control and amplify the bi-isotropic effects for the reflection and transmission of the considered nanoresonator systems. Furthermore, we use a "purely phenomenological" description of rather complicated (chiral, nonreciprocal, MM, ENZ) electromagnetic media with effective material parameters without specifying methods of their realization. The consideration of these methods and their features (e.g. account of spatial dispersion of the layered materials that can demonstrate properties of effective ENZ media [13,22–24]) goes beyond the present paper. However, these electromagnetic materials have been investigated for a long time, and various technologies to obtain and homogenize such materials (including also local analytical models for ENZ MMs) are sufficiently considered and experimentally confirmed (e.g., see [6–11,14,22,23] and numerous references in these works).

3 Main parameters and dependences for numerical analysis

The numerical analysis aims to investigate the characteristic properties of the reflected and transmitted radiation for subwavelength thicknesses of the layers or whole multilayer. At the same time, particular attention is paid to search the regimes of effective polarization conversion of the radiation. The detailed description of the analytical model and parameters (that were used for the numerical analysis below) were given in Section 2 of the previous paper [1]. In particular, the following complex values of parameters are used by default for the main layer material: dielectric permittivity, $\varepsilon_2 = 3 + 10^{-2}i$, magnetic permeability, $\mu_2 = 1.5 + 10^{-2}i$, chirality (α) and nonreciprocity (χ) parameters, $\alpha = (5/4)\,\chi = 5\cdot10^{-3}(1+i)$. Let us note that the choice of rather large α, χ values (that do not contradict the known restrictions on the α'', χ'' values for absorbing media [3,4]) is due to the requirement of clear visualization of the considered effects in the graphs below. However, the analyzed further effects also take place for smaller α, χ values. As the materials of the spacer layers, we use typical dielectric, ENZ, and metallic materials. We consider three types of the same materials of layers 1, 3 that will be called for brevity as: (i) "dielectric" layers, with parameters $\varepsilon_{1,3} = 4 + 0.01i$, $d_{1,3} = 0.15\,\mu m$; (ii) "ENZ" layers, $\varepsilon_{1,3} = 0.01 + 0.01i$, $d_{1,3} = 0.1\,\mu m$; (iii) "metallic" layers, $\varepsilon_{1,3} = -13 + 0.5i$, $d_{1,3} = 0.01\,\mu m$. For the numerical analysis, these materials are assumed to be nonmagnetic ($\mu_{1,3} = 1$). For all the cases, subwavelength thicknesses $d_1 = d_3$ are chosen for a given d_2 value and a material type to obtain the maximal effects of the spacer layers on the dependences under investigation. Also, we use the value $\lambda = 0.65\,\mu m$ for the incident wave wavelength. For all the figures, air is assumed to be the superstrate and substrate media ($\varepsilon_{0,4} = \mu_{0,4} = 1$), and the thicknesses of layers 1, 3 are equal ($d_1 = d_3$). The considered below effects also take place for the cases $\varepsilon_0 \neq \varepsilon_4$, $\mu_0 \neq \mu_4$, $d_1 \neq d_3$, and when changing quantities ε_2, μ_2, α, χ, $d_{1,2,3}$, λ in wide ranges. When the properties of the layers are different from the ones described above, the related values of parameters are given in captions to the figures below.

As basic quantities for the analysis, we consider $I_{r,t}$, $\tau_{r,t}$, $\theta_{r,t}$ that are relative intensities (intensities normalized to the incident wave intensity), ellipticities, and polarization azimuths, respectively, of the reflected and transmitted waves (to which low indexes r and t correspond), Figure 1. First of all, we investigate the dependences of $I_{r,t}$, $\tau_{r,t}$, $\theta_{r,t}$ on electromagnetic properties of the materials of layers 1, 2, 3, multilayer geometry (that is determined by thicknesses $d_{1,2,3}$), incidence angle (ψ_{in}) and polarization of the incident wave. All the angles in the graphs below (ψ_{in}, $\theta_{r,t}$) are calculated in the relative units of radians/π.

The data in Figure 2 illustrate characteristics of the reflected from and transmitted through the nanoresonator waves under the variation of dielectric properties of the spacer layers and the incident wave polarization (linear TM and TE polarizations are equivalent for the normal incidence, panels a, b). These data correspond to the properties of the field inside of the bi-isotropic layer

considered in Figure 6 of [1]. The changes of $\varepsilon'_{1,3}$ can significantly affect the quantities in the Figure 2 graphs. In all Figure 2 graphs, solid lines describe relative intensities $I_{r,t}$. The small values of the absorption parameters and thicknesses of the layers lead to the correspondence of the parameters $\varepsilon'_{1,3}$ ranges where low reflection and high transmission take place simultaneously.

The graphs for the polarization parameters of the reflected and transmitted waves ($\tau_{r,t}$, $\theta_{r,t}$) in all the panels of Figure 2, besides (b,c,d), can have resonance-like features for the definite ranges of $\varepsilon'_{1,3}$ values. The numerical analysis shows that these features (which determine, in particular, the cross-polarization effects for the reflected and transmitted waves [3,16,25]) are due to several reasons. The τ_r, θ_r peaks in panel (a) result from the nonreciprocity of the main layer material ($\chi \neq 0$). The peaks of $\tau_{r,t}$, $\theta_{r,t}$ in panels (e,f) are mainly determined by the chirality parameter ($\alpha \neq 0$). The resonance-like features in cases (g,h,l,m) take place also when $\alpha = \chi = 0$, so they are mainly caused by the complex mode structure of the field inside of the nanoresonator under the oblique incidence of the circularly polarized incident wave (see also Figs. 6d, f in [1]). The abrupt changes of quantities $\tau_{r,t}$, $\theta_{r,t}$ correspond, as a rule, to small values of I_r ($I_r \approx 0.01 \div 0.04$, panels (a,e, g,l)) and rather large values of I_t ($I_t \approx 0.8 \div 1$ at $\varepsilon'_{1,3} \approx 0$, panels (f,h,m)).

When changing the α' sign for the case in panel (b), angle θ_t also changes its sign, that is, the polarization plane of the transmitted wave rotates by the same angle to the opposite side. According to the used method to determine polarization characteristics (see the choice of angles $\theta_{r,t}$ in Fig. 1 and relations (21) of [1]), values $\theta_{r,t} < 0$ ($\theta_{r,t} > 0$) correspond to the right (left) rotation of the major axis of polarization ellipses (or to the polarization plane rotations for linearly polarized waves).

In going from the above considered data to the MM cases (the graphical data are not shown), the following basic effects take place. When $\varepsilon'_2 < 0$ ($\varepsilon'_2 = -3$, that corresponds to the proper wave parameters in Figure 7 of [1]), we have the condition $I_t \approx 0$ for all the data in Figure 2. Herewith, for the cases in panels (g,l), the abrupt changes of τ_r from 1 down to -1 (and vice versa) take place under the conditions $\varepsilon'_{1,3} \approx 0$, $I_r \approx 0.8 \div 0.9$. For the other MM case $\varepsilon'_2, \mu'_2 < 0$ ($\varepsilon'_2 = -3$, $\mu'_2 = -1.5$, that corresponds to the parameters of proper waves in Fig. 8 of [1]), differences of the peak structure of τ_r, θ_r are exhibited for cases (a,e). In this case, the other graphs are weakly changed in comparison with the ones in Figure 2.

4 Characteristic properties of reflected radiation

The dependences of the reflected wave characteristics on various parameters of the multilayer (materials and geometry) and the incident radiation (mainly, polarization and incidence angle) are given in Figures 3–6. The data in Figure 3 illustrate the dependences of the reflected wave relative intensity on the incidence angle for various
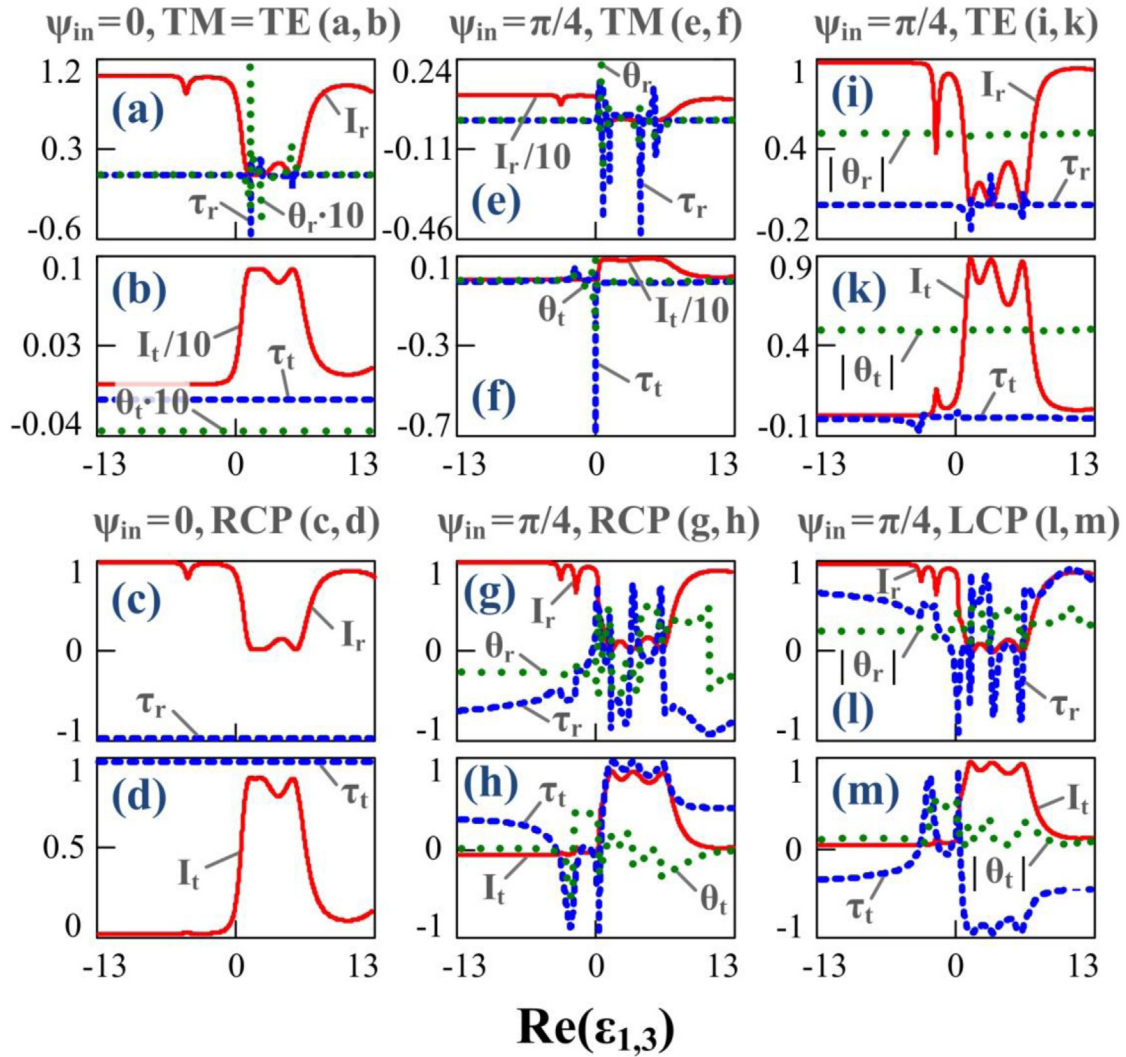
Fig. 2. The effect of the real part of the spacer layers permittivity on the parameters of reflected (I_r, τ_r, θ_r) and transmitted (I_t, τ_t, θ_t) waves ($\varepsilon'_{1,3}$ is used as the abscissa axis for all the graphs). The following values of parameters are used: $d_{1,3} = 0.15$ μm, $d_2 = 0.25$ μm, $\varepsilon''_{1,3} = 10^{-2}$, $\varepsilon_2 = 3 + 0.01i$, $\mu_2 = 1.5 + 0.01i$. The values of ψ_{in} and the incident wave polarization (RCP and LCP for right and left circular polarizations, here and below) are given above the corresponding graph panels. The other values of parameters correspond to the ones given in the main text (here and in the figures below).

polarizations of the exciting wave and properties of layers 1, 3.

It is seen that the spacer layers can lead to the significant changes in the dependences. The approximate analog of Brewster's effect can take place for all the considered polarizations (panels (a–c), d, (g–i) in Fig. 3). In these cases, the minimal I_r values are of the order of $10^{-4} \div 10^{-2}$. With that, the spacer layers (especially, for the case $d_{1,3} \neq 0$) can enable both the realization of the effect (panels (b,c,h,i)) and the pronounced shifts of Brewster's angle values (a,d,g).

Accounting for MM properties of the main layer material, the numerical analysis shows that the minimal differences from Figure 3 data take place when $\varepsilon'_2, \mu'_2 < 0$. In particular, in this case, the graphs are almost the same as in Figure 3 under the condition $d_{1,3} \neq 0$. For $\varepsilon'_2 = -3$, $\mu'_2 = 1.5$, the approximate Brewster effect is not practically

realized, though the pronounced minima of dependences $I_r(\psi_{in})$ can take place. In the latter case, the reflected wave is amplified, especially, for $\psi_{in} < \pi/4$. For all the considered cases (for the "conventional" and MM bi-isotropic layer), the graphs in Figure 3 are weakly changed (changes of I_r do not exceed 1–3%) when varying chirality and nonreciprocity parameters in the ranges $|\alpha|$, $|\chi| < 0.01$.

Let us consider the dependences of the reflected wave polarization (characterized by ellipticity τ_r and polarization azimuth θ_r, Fig. 1) on the system parameters (Figs. 4 and 5). The numerical analysis shows that dependences $\tau_r(\psi_{in})$, $\theta_r(\psi_{in})$ do not visually appear on the graphs for any combinations of the materials of layers 1, 3 (dielectric, ENZ, metallic) and incident TM or TE waves ($\tau_{in} = 0$) for the nonchiral and reciprocal main layer (the data are not given in the graphs). In this case, ellipticity and polarization azimuth of the reflected wave are determined
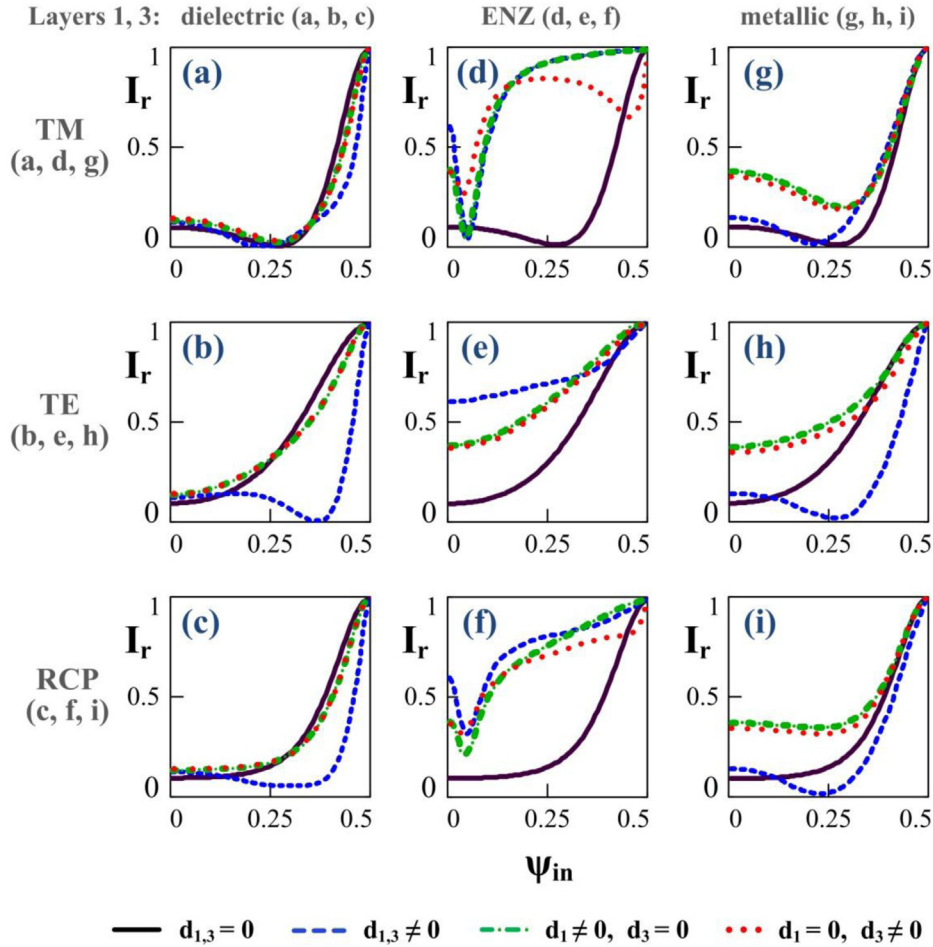
Fig. 3. The effect of the incidence angle on the reflected wave relative intensity for various exciting wave polarizations, geometries and materials of the spacer layers (here and below in similar figures, ψ_{in} is used as the abscissa axis for all the graphs).

by the ones for the incident wave, and these quantities do not practically depend on the incidence angle. For the circularly polarized (RCP, LCP) incident wave and the absence of layers 1, 3, dependences $\tau_r(\psi_{in})$ are near-to-linear (Figs. 4(a,c,e)), solid curves). At the same time, for normal incidence ($\psi_{in} = 0$), the reflected wave has the circular polarization, which is opposite to one for the incident wave, $\tau_r = -\tau_{in} = -1$. For the case of oblique incidence, at $\psi_{in} \to \pi/2$ the condition $\tau_r \to \tau_{in}$ is realized. When the spacer layers are absent ($d_{1,3} = 0$), quantity $|\theta_r|$ is decreased from value $\pi/2$ (obviously, that values $\theta_r = 0$, $\pi/2$ are physically undistinguishable) down to $\pi/4$, Figure 4 (b,d,f). For the presence of layers 1, 3 and circular polarization of the incident wave (Fig. 4, all the curves besides the solid ones), dependences $\tau_r(\psi_{in})$, $\theta_r(\psi_{in})$ can be nonlinear and characterized by the pronounced extrema. In this case, the significant effect on the polarization characteristics can be due to both double and single layers 1, 3, e.g. Figures 4 (c,d).

The numerical analysis also shows that the effect of layers 1, 3 on the reflected wave polarization is significantly weakened for the case $\varepsilon_2' < 0$. With that, dependences $\tau_r(\psi_{in})$ are similar to the ones in Figure 4 for the case $d_{1,3} = 0$, and the condition $\theta_r \approx -\pi/4$ takes place for wide ranges of ψ_{in}

(especially, for the dielectric or metallic spacer layers). When $\varepsilon_2', \mu_2' < 0$, the polarization characteristics under investigation are similar to the ones in Figure 4 for the case $d_{1,3} = 0$. As for the data considered in Figure 4, in this case, the effective conversion of the reflected wave polarization is realized.

When varying bi-isotropy parameters in wide ranges ($|\alpha|, |\chi| < 0.01$), including the cases of negative ε_2' or ε_2' and μ_2', the graphs in Figure 4, obtained for circular polarization of the incident radiation, have small changes (of the order of 1–2%). So, further, we consider the reflected wave polarization characteristics for the cases of the TM or TE incident wave (Fig. 5).

Data in Figure 5 illustrate the transformation of the reflected wave polarization (including the cross-polarization effects) for the chiral and reciprocal material of the main layer (for these data $\alpha = 5\cdot10^{-3}(1+i)$, $\chi = 0$), various materials of the spacer layers and the TM or TE polarized incident wave. In these cases, the pronounced nonlinear and resonance-like dependences $\tau_r(\psi_{in})$, $\theta_r(\psi_{in})$ can take place. To compare the polarization conversion regimes here and below, we consider the changes of quantities $\tau_{r,t}$ and $\theta_{r,t}$ (or $|\theta_{r,t}|$) when varying the incidence angle and other parameters of the system (in the first turn, the spacer layers geometry). These changes also describe the differences of
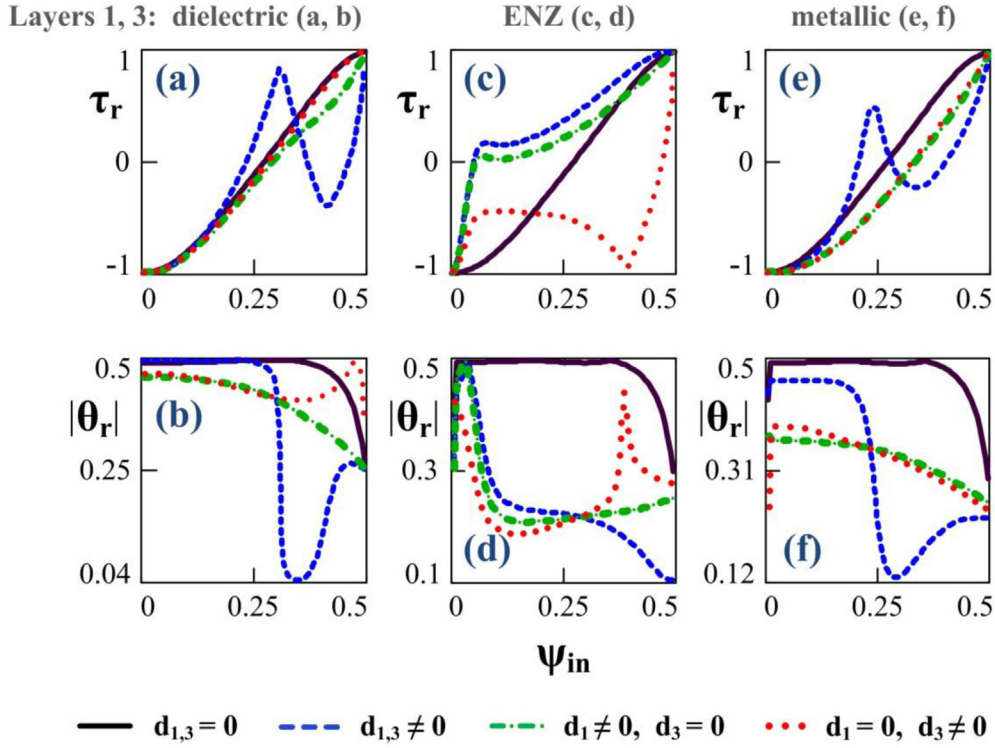
Fig. 4. Dependences of the reflected wave polarization parameters (ellipticity τ_r and polarization azimuth θ_r) on the incidence angle for RCP of the exciting wave ($\tau_{in} = 1$), various geometries and materials of the spacer layers.

parameters $\tau_{r,t}$, $\theta_{r,t}$ and the ones for the incident wave (τ_{in}, θ_{in}) in a number of cases below. The maximal changes of quantity τ_r ($\tau_r \approx 0.6 \div 0.7$) are realized for TM polarization in the case $d_{1,3} = 0$ (Fig. 5, the solid curves in panels (a,e,i)). For TE polarization, these values are $\tau_r \approx 0.2$ for dielectric layers 1, 3 and $\tau_r < 0.1$ for ENZ and metallic layers 1, 3 in the cases $d_{1,3} \neq 0$ (c,l) and $d_1 = 0$, $d_3 \neq 0$ (g).

The maximal changes of quantity $|\theta_r|$ ($|\theta_r| \approx 0.12\pi$) take place under the condition $d_{1,3} = 0$ for the TM incident wave, panels (b,f,k) in Figure 5. For the TE polarized incident wave, we have $|\theta_r| \approx 0.05\pi$ when $d_{1,3} \neq 0$ for dielectric layers 1, 3 (d) and $|\theta_r| < 0.01\pi$ for ENZ and metallic layers 1, 3 in the cases $d_{1,3} \neq 0$ (m) and $d_1 = 0$, $d_3 \neq 0$ (h). For many cases in Figure 5, the double spacer layers, creating nanoresonator configurations (when $d_{1,3} \neq 0$), determine (amplify) the transformation of the reflected wave polarization (especially, for the TE incident wave, panels (a–d,l,m)).

Some features of the data in Figure 5 take place under the additional variations of the parameters. For the chiral and nonreciprocal main layer material, a weakening of the considered polarization effects is realized for TM (TE) polarizations. Accounting for possible MM properties of the bi-isotropic layer, the following changes of the data in Figure 5 take place. In the case $\varepsilon_2' < 0$ ($\varepsilon_2' = -3$), dependences $\tau_r(\psi_{in})$, $\theta_r(\psi_{in})$ are practically absent for TM, TE polarizations of the incident wave and the considered materials of layers 1, 3. So, there is a peculiar suppression of the cross-polarization effects (for non-zero parameters α, χ), and this case is similar to the case of the nonchiral and reciprocal material of the main

layer. When $\varepsilon_2' = -3$, $\mu_2' = -1.5$, the corresponding graphs are similar to the ones in Figure 5 though the considered effects are slightly weakened (amplified) for the TM (TE) incident wave polarization.

Dependences $\tau_r(\psi_{in})$, $\theta_r(\psi_{in})$ in Figure 5 are strongly pronounced for rather large incidence angles ($\psi_{in} > 0.2\pi$). The comparison of the data in Figures 5 and 3 also shows that the considered polarization effects mainly take place under the conditions of the approximate realization of Brewster's effect for the nanoresonator when the reflected wave intensity is small ($I_r < 0.01 \div 0.02$). According to the numerical analysis, with increasing values of $|\alpha|$, $|\chi|$ (in compliance with the requirement of passivity of the main layer material [3,4]), the considered effects can be significantly amplified by choosing the spacer layers materials.

The reflection data (that correspond to the ones in Figs. 4, 5) for the case of the chiral EMNZ or chiral nihility material [26–28] of the main layer are given in Figure 6. The graphs in Figure 6 are obtained for metallic layers 1, 3 (similar results also take place for the ENZ or dielectric spacer layers). The graphs have features for small incidence angles. For $\psi_{in} \approx 0$, functions $I_r(\psi_{in})$ have the pronounced minima for various polarizations, Figures 6 (a,d,g). With growing ψ_{in} values, these functions increase up to values $I_r \approx 0.9$ and greater. For small ψ_{in}, the strong changes of the reflected wave polarization are realized, panels (b,c,e,f,h,i). At the same time, the significant (up to several tens of per cent) changes of τ_r and θ_r occur for a rather large reflection ($I_r \approx 0.1 \div 0.2$ and greater, especially, for double or single layers 1, 3). In particular, the considerable rotation of the
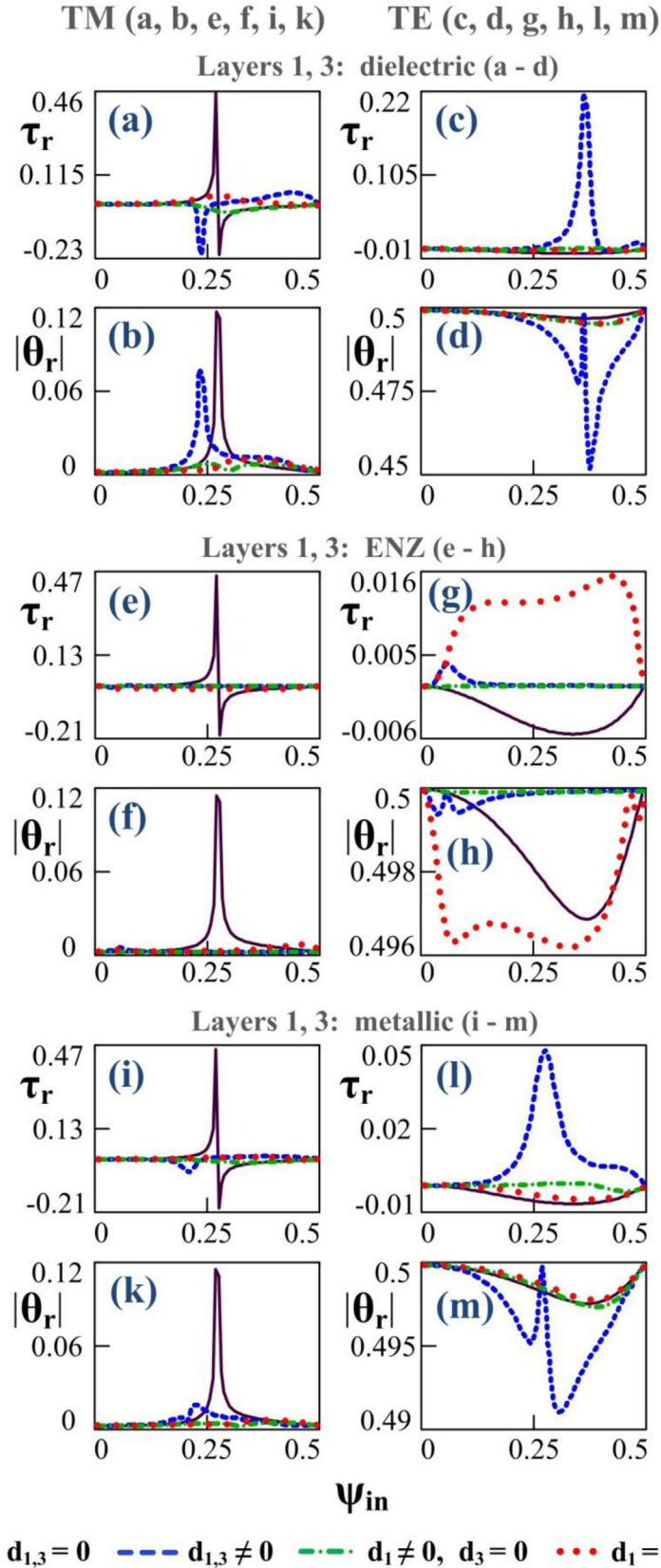
Fig. 5. Dependences of the reflected wave polarization parameters on the incidence angle for TM and TE polarizations of the exciting wave ($\tau_{in} = 0$), various geometries and materials of the spacer layers. $\chi = 0$.
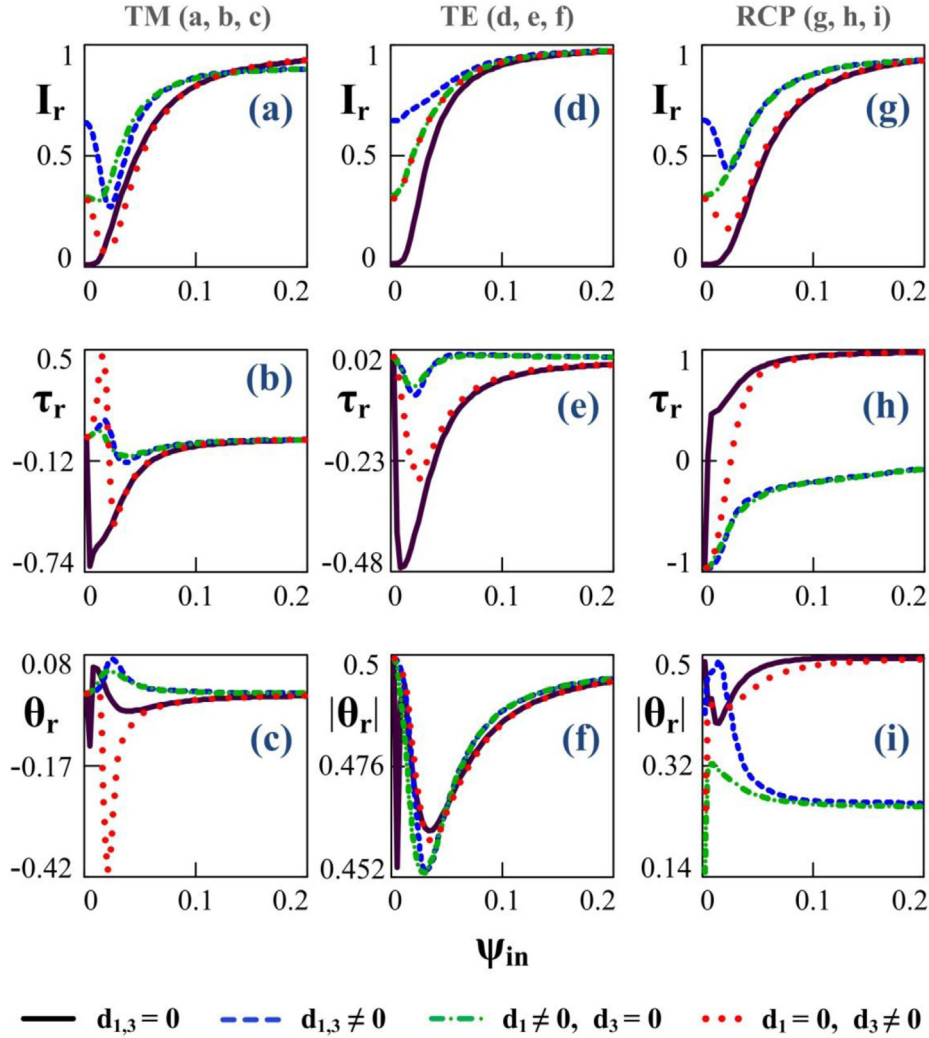
Fig. 6. Dependences of the relative intensity and polarization parameters of the reflected wave on the incidence angle for the EMNZ bi-isotropic layer, various geometries of the metallic spacer layers, and incident wave polarizations. The values of parameters $\varepsilon_2 = 0.01\,(1+i)$, $\mu_2 = 0.01 + 0.005i$, $\alpha = 0.005\,(1+i)$, $\chi = 0$ are used.

major axis of polarization ellipse for the TM or TE incident wave and the transition from the LCP to RCP (and vice versa) reflected wave are possible (panels (c,f) and (h), respectively).

The ψ_{in} ranges in Figure 6, when the strong polarization conversion takes place, correspond to the ones for the extreme dependences of birefringence and dichroism parameters of the field inside of the EMNZ bi-isotropic medium (see panels (d–i) in Figs. 3, 4 of [1]). So, according to the Figure 6 data, the significant modification of the reflected wave characteristics caused by the spacer layers takes place also in this case. The comparison of the data in Figures 4, 5 and 6 shows that in the latter case the values of τ_r, $|\theta_r|$, I_r can significantly exceed (e.g. on the order and

greater for the TM and TE polarizations) the ones for the case of the "conventional" bi-isotropic material of the main layer (Figs. 4 , 5).

According to the numerical analysis, the main layer material nonreciprocity (in the range of parameters $|\chi| < |\alpha|$) influences insignificantly $I_r(\psi_{in})$ graphs in Figure 6. However, $\tau_r(\psi_{in})$, $\theta_r(\psi_{in})$ graphs for TM and TE polarizations can have significant changes in this case (quantities τ_r, $|\theta_r|$, caused by nonreciprocity, can be of the order of 10–20% and greater, including cases of the corresponding increase of τ_r, $|\theta_r|$ values). Let us also note that the presence of dependences $\tau_r(\psi_{in})$, $\theta_r(\psi_{in})$ in the Figures 5, 6 data (for TM and TE polarizations) is due to chirality and nonreciprocity of the main layer material.
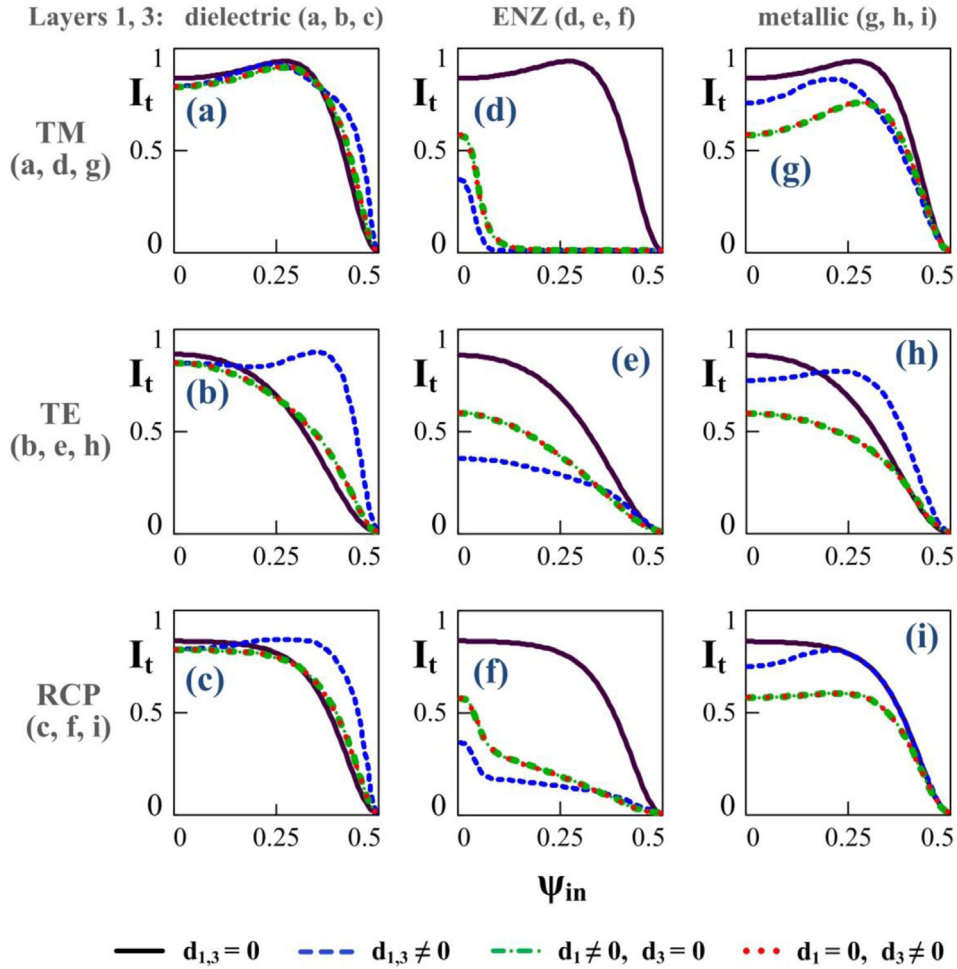
Fig. 7. The effect of the incidence angle on the transmitted wave relative intensity for various polarizations of the exciting wave, geometries and materials of the spacer layers.

These dependences are absent in the case $\alpha = \chi = 0$ when the reflected wave polarization corresponds to the one for the incident TM or TE wave.

5 Characteristic properties of transmitted radiation

The dependences of the transmitted wave relative intensity on the incidence angle for various exciting wave polarizations and spacer layers (that correspond to the Fig. 3 data for reflection) are given in Figure 7. The comparison of the graphs in Figures 3, 7 shows that the approximate relation $I_t \approx 1 - I_r$ takes place. So, the absorption of electromagnetic field energy inside of the multilayer is rather small. With that, a relative energy dissipation, $Q \approx 1 - I_r - I_t$, does not exceed values $0.1 \div 0.2$ for the cases in Figures 3, 7. Similar to the reflection case (Fig. 3), the spacer layers can significantly change dependences $I_t(\psi_{in})$ in Figure 7 (especially, when $d_{1,3} \neq 0$). The transmission maxima, as a rule, correspond to Brewster's angles for reflection (panels (a–c), (g–i) in Figs. 3, 7). However, for the

ENZ spacer layers, the approximate Brewster effect and $I_t(\psi_{in})$ maxima correspond to the slightly different incidence angles, panels (d,f) in Figures 3, 7. As for the reflected wave intensity (Fig. 3), the changes of I_t due to variation of parameters α, χ do not exceed 1–3% for the data in Figure 7.

Taking into account relation $I_t \approx 1 - I_r$, the effects of possible MM properties of the bi-isotropic layer material mainly correspond to the reflection features considered in Figure 3. In particular, the Figure 7 graphs are weakly changed under the transition to the case $\varepsilon_2', \mu_2' < 0$. In the case $\varepsilon_2' = -3$, $\mu_2' = 1.5$, dependences $I_t(\psi_{in})$ are very weak $(I_t \approx 10^{-4})$ for all the data in Figure 7.

The dependences of the transmitted wave polarization (described by ellipticity τ_t and polarization azimuth θ_t, Fig. 1) on the incidence angle for various parameters are given in Figures 8, 9. As for the reflection case (Fig. 4), there are practically no dependences $\tau_t(\psi_{in})$, $\theta_t(\psi_{in})$ ($\tau_t \approx \tau_{in}$, $\theta_t \approx \theta_{in}$ with high accuracy) for the case $\alpha = \chi = 0$, TM or TE linearly polarized incident wave and various materials of layers 1, 3. For the circularly polarized incident wave and the absence of layers 1, 3, functions $\tau_t(\psi_{in})$
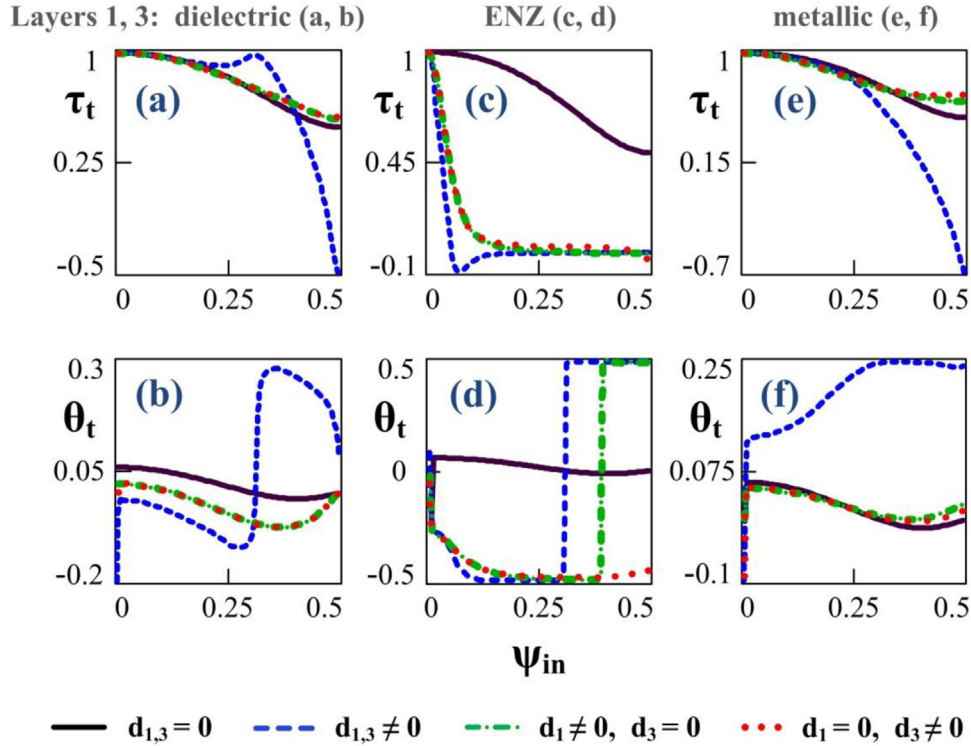
Fig. 8. Dependences of the transmitted wave polarization parameters on the incidence angle for RCP of the exciting wave ($\tau_{in} = 1$), various geometries and materials of the spacer layers.

are near-to-linear and decreasing in the range $\tau_t = 1 \div 0.5$ (the solid curves in panels (a,c,e) of Fig. 8). When $\psi_{in} = 0$, the transmitted wave polarization (RCP or LCP) corresponds to the one for the incident wave. The changes of θ_t are rather small for the case $d_{1,3} = 0$ (Figs. 8(b,d,f), the solid curves). The spacer layers provide the significant modification of the graphs of functions $\tau_t(\psi_{in})$, $\theta_t(\psi_{in})$, especially, when $d_{1,3} \neq 0$ for dielectric and metallic layers 1, 3 (Figs. 8(a,e,b,f)) and for all the cases of ENZ layers (Figs. 8(c,d)).

Under the condition $\varepsilon'_2, \mu'_2 < 0$ (the graphical data are not given) for all cases in Figure 8, besides the case $d_{1,3} \neq 0$, the graphs have similar features. At the same time, when $d_{1,3} \neq 0$, the considerable changes of the transmitted wave polarization take place for cases (a,b,e,f). As in the reflection case (Fig. 4), the variation of parameters α, χ in the ranges $|\alpha|, |\chi| < 0.01$ leads to the small changes of the graphs for all cases considered in Figure 8.

Figure 9 is a transmission "analogue" of Figure 5 (besides $\chi = 0$, the same other parameters are used). Dependences $\tau_t(\psi_{in})$, $\theta_t(\psi_{in})$ for the data in Figure 9 are absent at $\alpha = \chi = 0$ when the transmitted wave polarization corresponds to the one for the incident TM or TE wave. According to Figure 9, the spacer layers can significantly amplify polarization conversion of the transmitted radiation, especially, for rather large incidence angles ($\psi_{in} > \pi/4$). The maximal changes of ellipticity τ_t ($|\Delta\tau_t| \approx 1$) and polarization azimuth ($|\Delta\theta_t| \approx 0.5\pi$) (in comparison with the ones for the incident wave, τ_{in}, θ_{in}) under the variation of ψ_{in} take place for the TM polarization and ENZ layers 1, 3

(the cases $d_{1,3} \neq 0$ and $d_1 = 0$, $d_3 \neq 0$ in panels (e,f) of Fig. 9). For the remaining cases in Figure 9, values $|\Delta\tau_t| \approx 0.1$, $|\theta_t| \approx 0.02\pi$ and less are realized.

For the dielectric or metallic spacer layers, the corresponding graphs are qualitatively similar, panels (a–d) and (i–m), though the differences can take place for the separate cases, e.g. panels (c,d) and (l,m). As for the reflection case (Fig. 5), both double and single layers 1, 3 can amplify the polarization effects, e.g. panels (b,e,f,k,l) in Figure 9. The numerical analysis also shows that the main layer nonreciprocity (in the range of parameters $|\chi| < |\alpha|$) leads to the small changes of the Figure 9 graphs (the changes of τ_t, θ_t do not exceed 1–3%). The effects considered in Figure 9 also take place for the case $\varepsilon'_2, \mu'_2 < 0$ (with small decreases of $|\Delta\tau_t|$, $|\Delta\theta_t|$ values).

Figure 10 illustrates the transmitted wave properties (corresponding to the ones in Fig. 6) for the EMNZ bi-isotropic material of the main layer. It is seen, Figures 10 (a,d,g), that functions $I_t(\psi_{in})$ have the pronounced maximum for small incidence angles (in particular, at $\psi_{in} = 0$ for the case $d_{1,3} = 0$). With growing ψ_{in}, these functions are monotonically decreasing. As for the reflection case (Fig. 6), there are strong dependences $\tau_t(\psi_{in})$, $\theta_t(\psi_{in})$ with one or several extrema for small ψ_{in}, Figures 10(b,c,e,f,h,i). With that, the considerable changes of polarization parameters depending on ψ_{in} take place (up to values $|\Delta\tau_t| \approx 0.2 \div 0.4$, $|\Delta\theta_t| \approx 0.1\pi$ for TM or TE polarizations, panels (b,c,e,f), and $|\Delta\tau_t| \approx 0.9$, $|\theta_t| \approx 0.2\pi$ for RCP (h,i)).
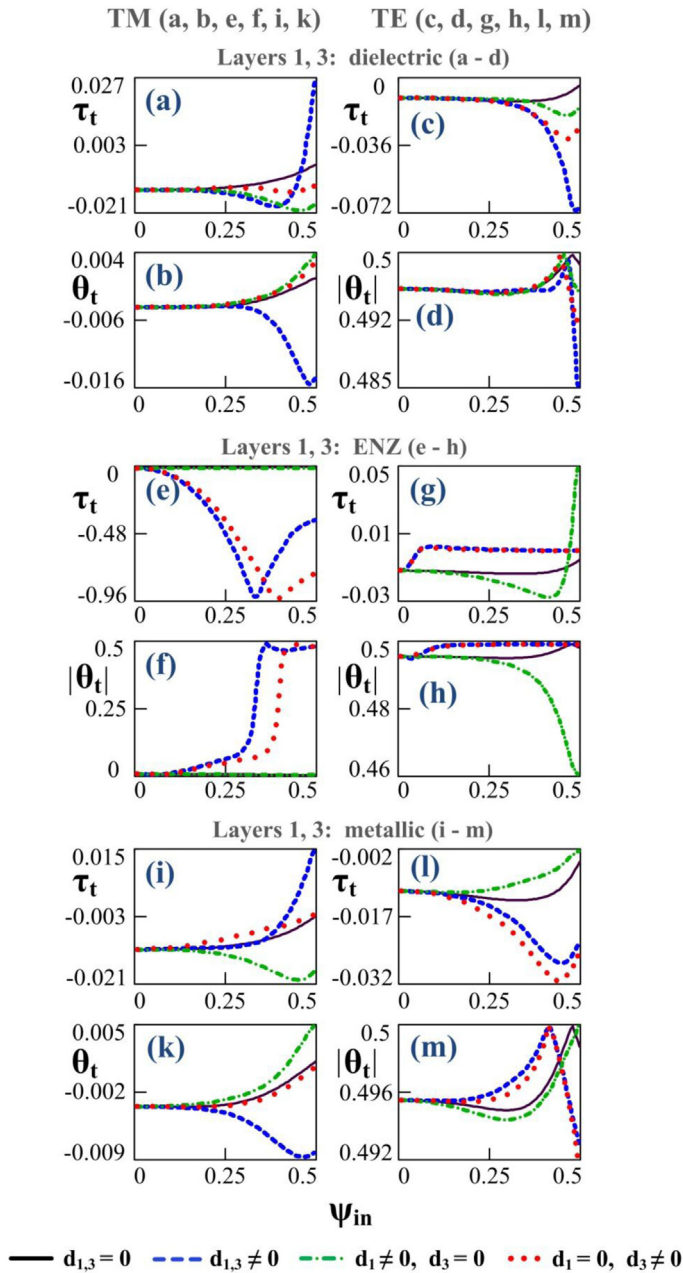
TM (a, b, e, f, i, k)   TE (c, d, g, h, l, m)

Fig. 9. Dependences of the transmitted wave polarization parameters on the incidence angle for TM and TE polarizations of the exciting wave ($\tau_{in} = 0$), various geometries and materials of the spacer layers. $\chi = 0$.

Comparing Figures 8–10, we see that quantities $|\Delta\tau_t|$, $|\theta_t|$ are significantly greater (on the two orders and more for TM and TE polarizations) than the ones in Figures 8 and 9. These polarization transformations can correspond to the rather high intensities ($I_t \approx 0.5$ and greater, especially, for the cases $d_1 \neq 0$ and (or) $d_3 \neq 0$). In particular, the RCP incident wave can be transformed into a near-linearly polarized transmitted wave, Figures 10(h,i). As for the reflection case (Fig. 6), the regimes of the strong amplification of polarization effects (due to the spacer

layers) are possible. The similar effects are also realized for the ENZ or dielectric spacer layers and for the case of chiral and reciprocal material of the main layer ($\chi = 0$).

The dependences of the transmitted radiation parameters (corresponding to the Fig. 10 data) on the relative thickness of the main layer, d_2/λ, where λ is the incident radiation wavelength, are given in Figure 11. It is interesting that the graphs in Figures 10 and 11 are very similar. So, the increase of ψ_{in} is approximately equivalent to the growth of d_2/λ for the considered parameter ranges. According to the data in Figure 11, conditions $0 < \psi_{in} < 0.05\pi$, $d_2/\lambda < 0.5$ are rather optimal for the polarization conversion. In doing so, values $I_t > 0.1 \div 0.2$ (panels (a,d,g) in Fig. 11), $|\tau_t| \approx 0.6 \div 1$, $|\Delta\theta_t| \approx (0.1 \div 0.3)\,\pi$ (b,c,e,f,h,i) take place. In this case, the spacer layers can lead to the significant modification of the transmitted wave polarization, especially, for the cases $d_{1,3} \neq 0$ and $d_1 = 0$, $d_3 \neq 0$. Let us note that the EMNZ bi-isotropic main layer suppresses the multibeam interference effects (that are similar to the ones considered in [1]) for dependences $I_t(d_2/\lambda)$.

Some changes of Figure 11 data under the parameter variations were also considered (the graphical data were not represented). For the case of the near to normal incidence ($\psi_{in} \approx 0$), the dependences for quantities τ_t, θ_t in Figure 11 become near to linear and weakly decreasing ($|\Delta\tau_t| < 0.05$, $|\Delta\theta_t| < 0.02\pi$) for TM or TE incident wave, and condition $\tau_t \approx \tau_{in}$ takes place for the circular polarization. Similar features also take place for the "conventional" (non-EMNZ) bi-isotropic main layer (for $\varepsilon'_2, \mu'_2 > 1$) under both the normal and oblique incidence.

6 Conclusion

The executed numerical modeling, based on the previous analytical results [1], generally confirms the idea to apply the considered subwavelength multilayer systems (as a rule, in the nanoresonator configurations), including the main bi-isotropic layer sandwiched between the spacer layers of various "conventional" or ENZ materials, for the control and amplification of chiroptical response in nanophotonics devices, effective polarization conversion. In particular, such nanoresonators can transform the incident electromagnetic wave with linear or circular polarization into the output waves with various polarization parameters.

The results of the numerical analysis have shown the main features of the reflection and transmission in the investigated systems. The energy and polarization characteristics of the reflected and transmitted waves can depend significantly on the electromagnetic properties and geometry of the spacer layers (the dielectric, ENZ, and metallic ones, with the thicknesses of the order of hundreds and tens of nanometers, respectively, Figs. 2, 3, 7). The dependences of energy ($I_{r,t}$) and polarization ($\tau_{r,t}$, $\theta_{r,t}$) characteristics of the radiation on the incidence angle (ψ_{in}) have been investigated in detail (Figs. 3–10). For the linear (TM or TE) polarizations of the exciting wave, the following main features take place: (i) the resonance-like dependences $\tau_r(\psi_{in})$, $\theta_r(\psi_{in})$ for the ψ_{in} ranges correspond-
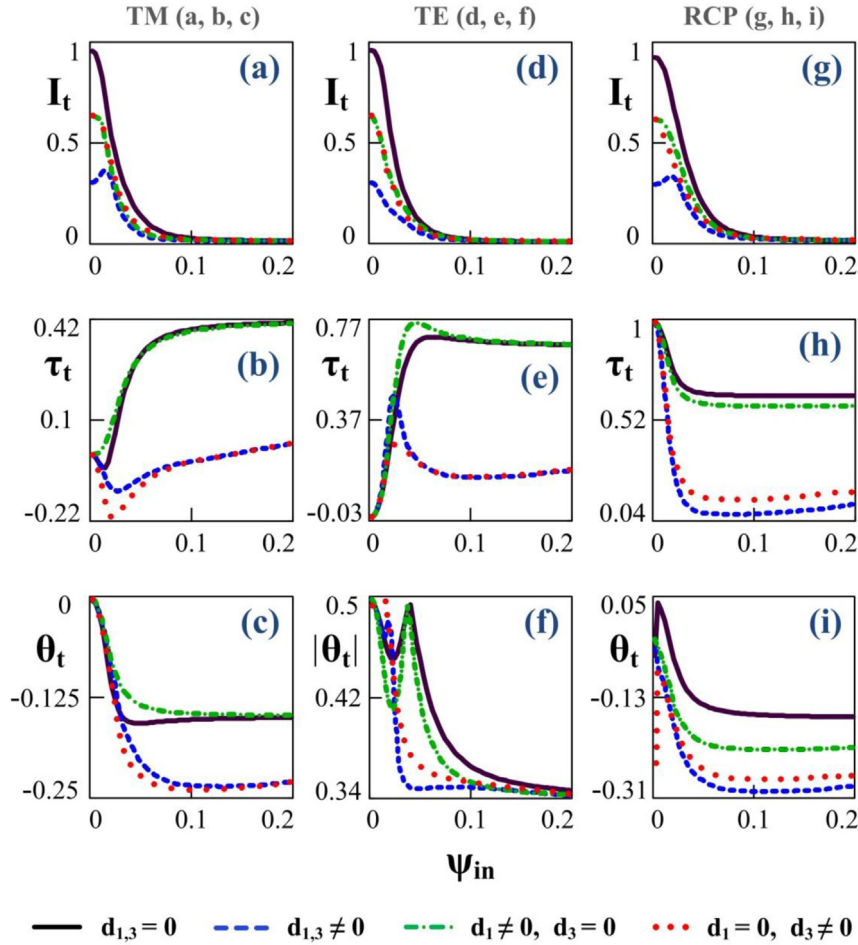
Fig. 10. Dependences of the relative intensity and polarization parameters of the transmitted wave on the incidence angle for the EMNZ bi-isotropic main layer, various geometries of the metallic spacer layers, and incident wave polarizations. The parameters $\varepsilon_2 = 0.01\,(1 + i)$, $\mu_2 = 0.01 + 0.005i$ are used.

ing to the approximate realization of Brewster's effect ($I_r < 0.01 \div 0.02$, Fig. 5); (ii) the strong non-linear dependences $\tau_t(\psi_{in})$, $\theta_t(\psi_{in})$, especially, for values $\psi_{in} \geq \pi/4$ when $I_t < 0.8 \div 0.9$ (Fig. 9). Under the usually realizable condition $|\varepsilon_2|$, $|\mu_2| \gg |\alpha|$, $|\chi|$, the $I_{r,t}$ changes due to the used values of chirality and nonreciprocity parameters are not exceed 1–3%. Parameters α, χ affect functions $\tau_{r,t}(\psi_{in})$, $\theta_{r,t}(\psi_{in})$ stronger for the linearly polarized exciting wave. As a rule, the chirality effects on the polarization characteristics (more pronounced for the transmitted radiation) are the most significant in comparison with the nonreciprocity effects.

The effects of various MM multilayer components on the reflection and transmission have been considered. In particular, in the transition from the "conventional" bi-isotropic layer $(\varepsilon_2', \mu_2' > 0)$ to the double-negative MM one $(\varepsilon_2', \mu_2' < 0)$, the output wave intensities (e.g. dependences $I_{r,t}(\psi_{in})$) are weakly changed. However, the polarizations and wave vectors of these waves can be much more "sensitive" to such a transition (see also [1]). So, the corresponding polarization effects can be used to identify

the MM effective properties of chiral and bi-isotropic nanocomposites. With that, MM properties of the main layer material can both weaken (e.g. when $\varepsilon_2' \mu_2' < 0$) and amplify the chiral and nonreciprocal effects.

Rather optimal conditions to transform polarization of the reflected or transmitted radiation (when quantities $I_{r,t}$ and changes of $\tau_{r,t}$, $\theta_{r,t}$ are maximal under variation of the system parameters and in comparison with the ones for the incident wave) are provided for the EMNZ bi-isotropic (in particular, EMNZ chiral or chiral nihility) material of the main layer. In these cases, the changes of polarization parameters, e.g. for the oblique incidence $(\psi_{in} < 0.2\pi)$ of TM or TE polarized incident waves, are of the order of $|\Delta\tau_r| \approx 0.7$, $|\Delta\theta_r| \approx 0.4\pi$ and $|\Delta\tau_t| \approx 0.8$, $|\Delta\theta_t| \approx 0.2\pi$ for relative intensities $I_r > 0.1 \div 0.2$ and $I_t > 0.5$, respectively, and subwavelength thicknesses of the system (Figs 6, 10, 11). These $|\Delta\tau_t|$, $|\Delta\theta_t|$ values can exceed significantly (on the one (two) order(s) and more for the reflection (transmission), correspondingly) the ones for the cases of the "conventional" (non-EMNZ) bi-isotropic or chiral main layer.
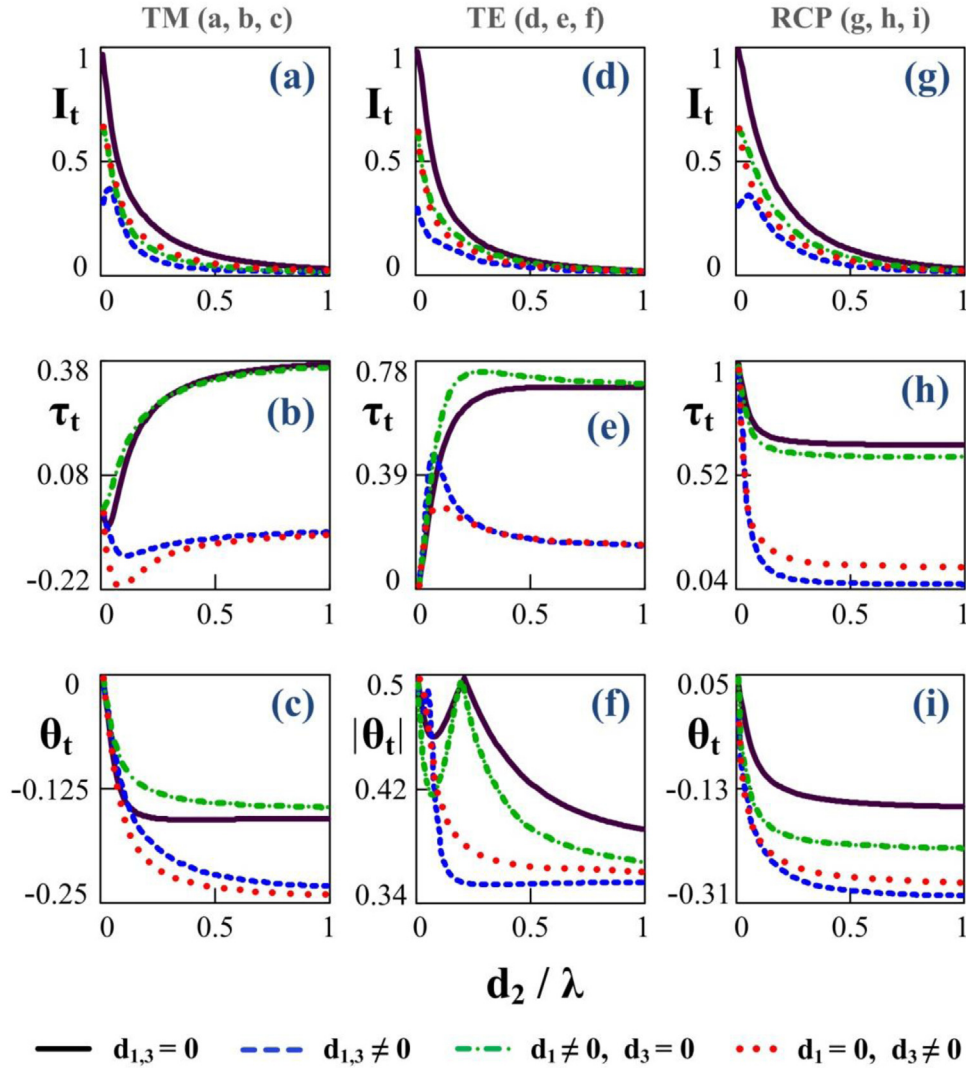
Fig. 11. Dependences of the relative intensity and polarization parameters of the transmitted wave on the main layer relative thickness for the EMNZ bi-isotropic main layer, various geometries of the metallic spacer layers, and incident wave polarizations. The values of parameters correspond to Figure 10. $\psi_{in} = 0.05\pi$.

For the majority of the considered multilayer and incident wave parameters, the presence, variation of the materials and geometry of the spacer layers (especially, for the nanoresonator configurations) can provide the manifold opportunities to control and amplify the investigated (mainly, polarization) effects. Let us note that these effects can be considerably amplified for the thin bi-isotropic layer with the larger values of chirality and nonreciprocity parameters (that can be obtained using various approaches [29–34]) and applying modern optimization methods (e.g. [35,36]) to search desired parameters of the system. Furthermore, various approaches to reduce the size of chiral or bi-isotropic inclusions and nanoparticles in nanocomposites down to the size of separate molecules are actively developed (e.g. [6–9, 37–39]). The considered characteristic properties of polarization conversion in the bi-isotropic systems can take place for multiple devices on the basis of the investigated

nanoresonators or their modifications. The proposed concept can be simply scaled for wide (not only optical) frequency ranges of coherent radiation and various types of the multilayer components. The obtained results (together with the ones in [1]) can be also relevant to the modeling and development of metasurfaces, polarization converters with reduced volumes of active material, ultrathin polarization modulators, chiral sensors, nanophotonics components of chiroptical spectroscopy and data processing systems.

References

1. E. Starodubtsev, J. Electromagn. Waves and Appl. **36**, 2647 (2022)
2. F.I. Fedorov, Theory of Gyrotropy (Nauka i Tehnika, Minsk (in Russian), 1976)

3. I.V. Lindell, A.H. Sihvola, S.A. Tretyakov, A.J. Viitanen, Electromagnetic Waves in Chiral and Bi-isotropic Media (Norwood, MA: Artech House, 1994)

4. I.V. Lindell, Methods for Electromagnetic Field Analysis, 2nd edn. (IEEE Press, New York, 1995)

5. A. Serdyukov, I. Semchenko, S. Tretyakov, A. Sihvola, Electromagnetics of Bi-Anisotropic materials, Theory and Applications (Routledge, Evanston, IL, 2001)

6. Z. Wang, F. Cheng, T.G. Winsor et al., Nanotechnology **27**, 412001 (2016)

7. J. Mun, M. Kim, Y. Yang et al., Light Sci. Appl. **9**, 139 (2020)

8. X. Ma, M. Pu, X. Li et al., Nanomaterials **7**, 116 (2017)

9. S. Oh, O. Hess, Nano Convergence **2**, 24 (2015)

10. E. Ashalley, C.-P. Ma, Y.-S. Zhu et al., J. Electr. Sci. Technol. **19**, 100098 (2021)

11. C.M. Soukoulis, M. Wegener, Nat. Photonics. **5**, 523 (2011)

12. N. Yu, F. Capasso, Nat. Mater. **13**, 139 (2014)

13. C. Rizza, A. Di Falco, M. Scalora et al., Phys. Rev. Lett. **115**, 057401 (2015)

14. S. Jahani, Z. Jacob, Nat. Nanotechnol. **11**, 23 (2016)

15. V.-C. Su, C.H. Chu, G. Sun et al., Opt. Express **26**, 13148 (2018)

16. V.S. Asadchy, A. Diaz-Rubio, S.A. Tretyakov, Nanophotonics **7**, 1069 (2018)

17. S. Yoo, Q.-H. Park, Nanophotonics **8**, 249 (2019)

18. E.G. Starodubtsev, Mater. Res. Express **5**, 1 (2018)

19. E. Starodubtsev, EPJ Appl. Metamat. **6**, 22 (2019)

20. E. Starodubtsev, EPJ Appl. Metamat. **7**, 1 (2020)

21. E. Starodubtsev, J. Electromagn. Waves Appl. **35**, 766 (2021)

22. D. Yoo, F. Vidal-Codina, C. Ciraci et al., Nat. Commun. **10**, 4476 (2019)

23. N. Kinsey, C. DeVault, A. Boltasseva et al., Nat. Rev. Mat. **4**, 742 (2019)

24. M. Gorlach, M. Lapine, Phys. Rev. B. **101**, 075127 (2020)

25. D.G. Sannikov, Techn. Phys. Lett. **35**, 352 (2009)

26. S. Tretyakov, I. Nefedov, A. Sihvola et al., J. Electromagn. Waves Appl. **17**, 695 (2003)

27. Y. Ra'di, V.S. Asadchy, S.A. Tretyakov, EPJ Appl. Metamat. **2**, 1 (2015)

28. I. Liberal, N. Engheta, Nat. Photonics **11**, 149 (2017)

29. Do-H. Kwon, D.H. Werner, A.V. Kildishev et al., Opt. Express **16**, 11822 (2008)

30. V.K. Valev, J.J. Baumberg, C. Sibilia et al., Adv. Mater. **25**, 2517 (2013)

31. J.T. Collins, C. Kuppe, D.C. Hooper et al., Adv. Opt. Mater. **5**, 1700182 (2017)

32. C. Kilchoer, N. Abdollahi, J.A. Dolan et al., Adv. Opt. Mater. **8**, 1902031 (2020)

33. A. Ali, A. Mitra, B. Aissa, Nanomaterials **12**, 1027 (2022)

34. J. Wang, Y.J. Liu, H.Y. Dong et al., Phys. Rev. Res. **4**, 013147 (2022)

35. A.V. Kildishev, U.K. Chettiar, Z. Liu et al., JOSA B **24**, A34 (2007)

36. P.-Y. Chen, C-H. Chen, H. Wang et al., Opt. Express **16**, 12806 (2008)

37. A. Adawy, Symmetry **14**, 292 (2022)

38. M. Ma, J. Chen, H. Lin et al., Nanoscale **14**, 13405 (2022)

39. M.A. Hubbard, C. Luyet, P. Kumar et al., Chirality **12**, 1494 (2022)